JOURNAL OF MATERIALS SCIENCE **33** (1998) 5301–5309

Microstructure evolution and grain growth in the sintering of 3Y–TZP ceramics

J. LUO, S. ADAK*, R. STEVENS
Department of Materials Science and Engineering, University of Bath, Bath BA2 7AY, UK

Microstructural evolution and grain growth in 3Y–TZP ceramics have been examined using two nano-sized 3Y–TZP powders, calcined at different temperatures, derived from the same hydroxide powder. The green bodies prepared from both powders showed two sets of porosity: inter-agglomerate and intra-agglomerate. The intra-agglomerate pores are related to initial crystallite size; the size of the inter-agglomerate pores are governed by the pressure applied to the green bodies. Due to the nano-sized dimensions, the intra-agglomerate porosity has little effect on the final density and grain size. In contrast, the large inter-agglomerate pores play a major role on both the sintering process and achievement of final density. During sintering, the grains initially grew to approximately 100 nm, reaching the intermediate stage of sintering; the grain growth rate then became very much reduced before reaching the final stage of the sintering process. At this point, significant grain growth took place, possibly controlled by the solution drag mechanism. The activation energy for the grain growth was determined to be 352 kJ/mol.

1. Introduction

3Y–TZP ceramics have become more commercially important as engineering materials due to their high mechanical properties and a coefficient of thermal expansion similar to steels. Specific mechanical properties of 3Y–TZP are very sensitive to the microstructure. In general, fine and uniform grain structure with full density is required for engineering ceramics to achieve good mechanical properties. 3Y–TZP is even more sensitive to grain size because the martensitic transformation of tetragonal and monoclinic phases, which has a predominant effect on the mechanical properties, is again sensitive to grain size. 3Y–TZP ceramics with uniform sub-micron grain size usually have good mechanical properties (i.e., high strength and toughness), which can be achieved by sintering commercially available nano-sized 3Y–TZP powder. In fact, specially prepared nano-sized 3Y–TZP powder can be densified at temperatures as low as 1000 °C. [1–4], but the final density depends on the characteristics of the starting powder, particularly agglomerate size. Due to the high specific surface energy of nano-sized powder, agglomeration readily occurs in the powder; consequently, it is difficult to sinter the material to theoretical density at low temperature by pressureless sintering. Hot-pressing or sintering-forging [3] can be used to obtain the fully dense material. The simplest and most commonly used method is to increase the sintering temperature.

Agglomeration in the starting powder, often in the spray-dried form, is one of the most important factors affecting the sintering and final density in zirconia ceramics [3, 5–7]. Adjacent particles within agglomerates first sinter together. The grains of the sintered parts grow and rearrange with subsequent increase in densification. Powder preparation techniques can determine the characteristics of the agglomerates [5, 7], thus affecting the sintering behavior of the powder. Dopants or impurities such as SiO_2, Al_2O_3, CuO, Fe_2O_3, etc., even in small quantities, will also affect the sintering by segregating at grain boundary and forming a grain boundary phase, usually a glassy phase, in combination with Y_2O_3 and ZrO_2 [8–12].

The grain-growth mechanism is also important during the sintering because the mechanical properties are very sensitive to the grain size in 3Y–TZP. Ruiz and Readey [13] reported that significant grain growth in 3Y–TZP ceramics took place at high-temperature heat treatment. Nightingale *et al.* [14] showed that grain-growth mechanism in 3Y–TZP during microwave sintering differed from that obtained by conventional pressureless sintering. Winnubst, Burggraaf, and colleagues [2, 15, 16] investigated the grain growth of 3Y–TZP ceramics during conventional pressureless sintering, their investigation being concentrated mainly on the initial and intermediate sintering stages. It is important to understand the science underlying the sintering mechanisms and microstructure evolution, but the properties are determined by the final microstructure. The final grain size is therefore significant and is generated mainly by the grain growth that occurs during the

* On secondment from the Department of Ceramic Engineering, Regional Engineering College, Rourkela 769 008, India.

final sintering stage. The grain-growth mechanism in the final stage of sintering, which was attributed to the solute drag mechanism [17], is usually different from that of the first two stages. In the present study, the microstructural evolution and grain growth have been characterized during the sintering of two nano-sized 3Y–TZP powders, which were prepared especially to demonstrate different behavior.

2. Experimental procedure

Yttria-doped zirconium hydroxide (MEL Chemicals, Manchester, UK) was used as the starting material. Two ZrO_2–3 mol % Y_2O_3 powders were obtained by calcining the hydroxide at two different temperatures, 650 °C and 900 °C, for 4 h. Crystallization phenomena were followed and crystallite size of the powders determined by X-ray diffraction (XRD) and transmission electron microscopy (TEM). Green bodies were made from the two powders by die pressing (50 MPa pressure) and/or followed by cold isostatic pressing (100 MPa pressure) for densification and grain-growth experiments. Mercury porosimetry was used to measure the porosity content and pore size distributions in the resultant green bodies. The sintering temperatures used were between 1250–1400 °C with dwell times of 1–64 h in air. Dilatometry measurements were also carried out to monitor the densification of the two powders. The densities of the fired sample were measured using the water immersion technique. The microstructures, grain size and porosity, of the fired samples were examined by scanning electron microscopy (SEM) on the polished and thermally etched surfaces. The grain size was determined using a rectangular intercept procedure, following the ASTM E112-88 standard. The average grain size, G, is then given by

$$G = \sqrt{\frac{4A}{\pi(n_i + n_o/2)}} \quad (1)$$

where A is the area of rectangular, n_i and n_o are the grain numbers in the rectangular and on the rectangular boundary, respectively.

3. RESULTS

3.1. Powder and powder compacts

Both the powders, calcined at 650 °C (powder-650) and 900 °C (powder-900), were examined by means of TEM (Fig. 1). The powders are in the form of agglomerates of nano-sized crystallites, and the agglomerates were clearly apparent in both the powders. Point contacts and necks can be seen to have formed between adjacent individual particles. No significant difference in agglomerate size was observed by TEM between powder-650 and powder-900, but the difference in crystallite size is obvious. Both TEM observation and XRD line broadening were used to determine the crystallite sizes of the powders, and the average sizes are 20 nm and 35 nm for powder-650 and powder-900, respectively.

The green densities of the powder compacts are 23.1% and 25.5% for powder-650 and -900, respectively, under die pressing (DP) at a pressure of 50 MPa (these samples are hereafter denoted as DP-650 and DP-900). Cold isostatically pressed (CIP, at a pressure of 100 MPa) compacts improve green densities to 32.6% and 35.5% for powder-650 and powder-900, respectively (these samples are hereafter denoted as CIP-650 and CIP-900). The difference in green density can be attributed to the finer crystallites of powder-650. Although in most commercial 3Y–TZP powder, the green density after CIP reaches 50% of theoretical density, the green density is very low for the nano-sized zirconia powder, due to less efficient packing when prepared at a pressure of 100 MPa or below [5, 16]. A much higher pressure is required to increase the green density further for a nano-sized powder [1].

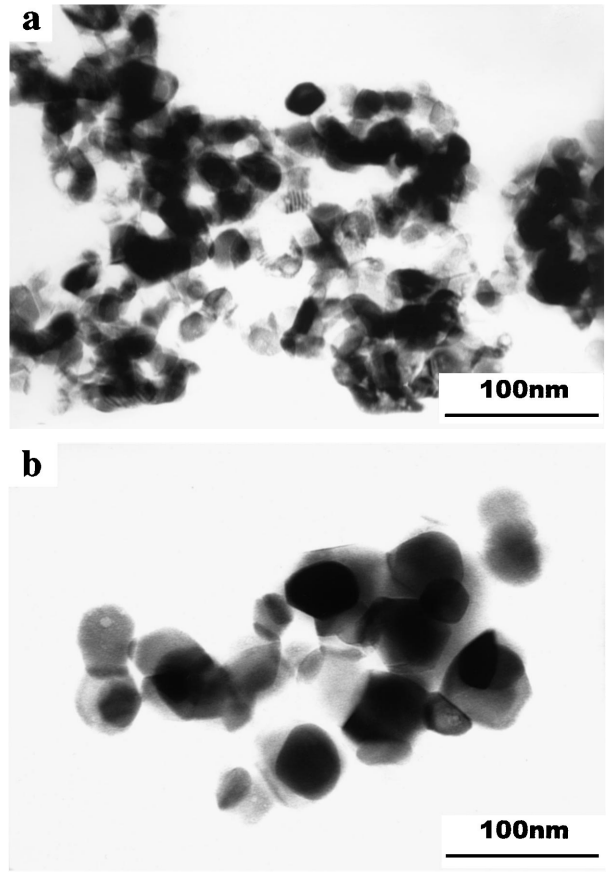

Figure 1 TEM observation of 3Y–TZP powder: (a) powder-650, calcined at 650 °C for 4 h; (b) powder-900, calcined at 900 °C for 4 h.

Fig. 2 shows the porosity distribution in the green bodies. As can be seen, there are two main peaks on the trace of all four samples. The first peak (very fine pores) is formed by occlusion of space by the particles in the agglomerates and is therefore related to the particle size. Powder-650 has an average particle size of 20 nm, and the average pore size formed by the particles is 8 nm, whereas powder-900 has an average particle size of 35 nm, and the average pore size is 17 nm. The pore size formed by the particles of both powders was not affected by green body formation techniques and pressure (see the comparison of DP-650 and CIP-650, and DP-900 and CIP-900). The second peak in the porosity trace is attributed to occlusion of space by the agglomerates. For hard agglomerates, the pore size mainly depends on the agglomerate size, but for soft agglomerates, which

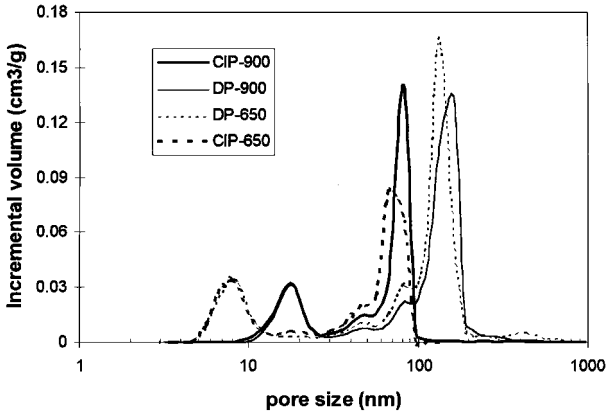

Figure 2 The porosity distributions in the green bodies, prepared by die pressing at pressure of 50 MPa (DP-650, and DP-900) and followed by cold isostatic pressing at pressure of 100 MPa (CIP-650 and CIP-900).

can be broken down, reducing the occluded space, the pore size also depends on the pressure [5, 7]. The pore size formed by agglomerates in this case is affected by the pressure used to form the green bodies. For bodies formed by CIP at pressure of 100 MPa, the average pore size is 80 nm, but for those formed by DP at pressure of 50 MPa, the average pore size is 160 nm. The pores formed by the agglomerates show no significant difference in size and distribution between powder-650 and powder-900, which indicates that the characteristics of the agglomerates are similar between powder-650 and powder-900. This was confirmed by TEM observation.

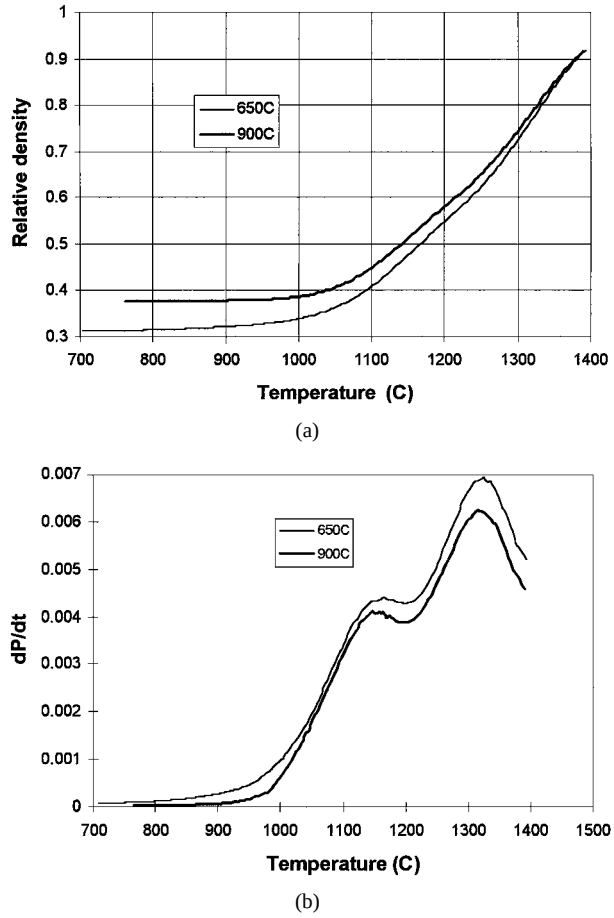

Figure 3 Densification of CIP-650 and CIP-900 during heating obtained bydilatometry: (a) relative density versus temperature; (b) densification rate versus temperature.

3.2. Dilatometric results

Dilatometric experiments were carried out to monitor the densification of the two powders (CIP-650 and CIP-900). Fig. 3a and b show the densification characteristics during the heating up cycle to 1400 °C. Fig. 3 shows that the densification of powder-650 starts at around 800 °C. The rate of sintering is very slow up to 1000 °C, and above this temperature, significant shrinkage starts to take place. While the sintering for powder-900 starts at 950 °C, it increases at temperature slightly higher than 1000 °C. The difference in sintering start-temperature between powder-650 and powder-900 can be attributed to the difference in crystallite size [3, 12].

As can be seen from Fig. 3b, there are two peaks in the plot of rate of change in relative density ($d\rho/dt$) against temperature for both the powders. Moreover, the peak positions for both powders are the same, corresponding to 1150 and 1330 °C. The two peaks can be ascribed to the different nature of the size distribution of the pores due to agglomerates present in the powder, inter- and intra-agglomerate, (Fig. 2). This phenomenon has been widely observed in fine zirconia powders [3, 5–7]. In the initial stage of sintering, the crystallites in each agglomerate are first sintered and densified at a high rate due to the "energetic, sinter-active" nano-sized crystallites. Sintering also takes place at contact points between agglomerates. Hence, rapid shrinkage accompanying sintering of the agglomerates will produce a tensile stress between adjacent agglomerates. This stress, if sufficiently large, can break away the sintered agglomerates from the surrounding matrix, leaving a gap that cannot then be closed by subsequent sintering; $d\rho/dt$ shows a minima at 1200 °C, corresponding to the transition temperature. An increased temperature is required to drive the sintering further to produce an increased density.

3.3. Effect of time and temperature on densification

Dilatometric results of both the powders showed that densification below 1000 °C was slow and that the density obtained is about 60% theoretical density at 1200 °C (Fig. 3). Further increase of temperature up to 1400 °C shows good densification. For the further investigation on the densification, powder compacts were sintered at 1250 to 1400 °C for different dwell times. To study the effect of the two sets of porosity (inter- and intra-agglomerate pores), two powder compacts were prepared for the densification investigations: one by die pressing (DP-650 and DP-900), the other by cold isostatic pressing (CIP-650 and CIP-900). Densities of the sintered materials plotted against time at different temperatures, for the powders 650 and 900, are shown in Fig. 4. There is no clear difference in densification behavior, for any of the sintering conditions, between powder-650 and powder-900, even though the crystallite size of the two powders is so different. As shown

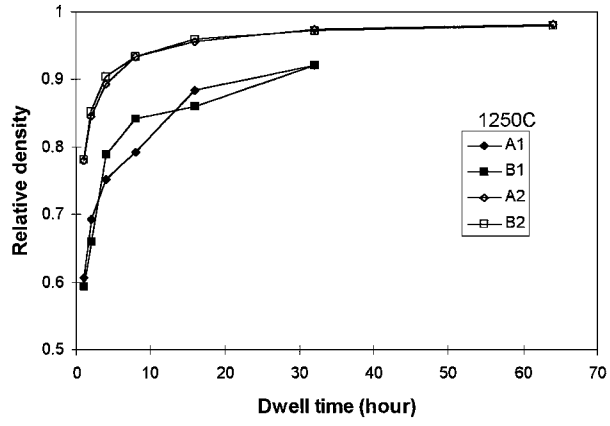

(a)

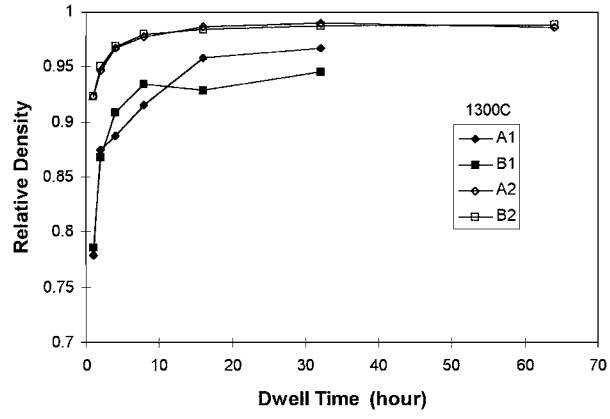

(b)

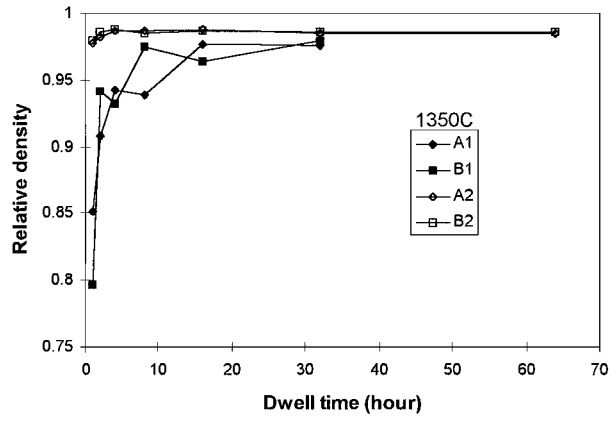

(c)

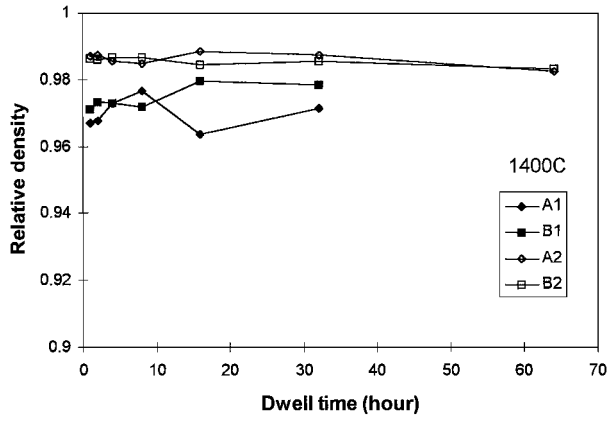

(d)

Figure 4 The relationship of dwell time on the densities of the four samples (DP-650, DP-900, CIP-650, and CIP-900) at four sintering temperatures: (a) 1250 °C; (b) 1300 °C; (c) 1350 °C; and (d) 1400 °C.

earlier, the densification curves obtained from dilatometric experiments are also similar between powder-650 and powder-900. This implies that either the crystallite size is not the predominant controlling factor for sintering for this case or that the small pores formed by the occluding particles can be easily eliminated at low temperatures and that they have no significant effect on the densification (Fig. 2). In view of the volume they occupy and the fact that they are eliminated early in the sintering process, this result is not unexpected. However, there is a significant difference observed in densification between the DP samples and the CIP samples. The CIP powder compact can be densified at relatively low temperatures and shorter times. The DP samples always have lower density than the CIP samples after similar sintering conditions, even after sintering at 1400 °C, where densification is complete and the main phenomenon is grain growth. In this case, densities of 97.5% and 98.5% are achieved for the DP and CIP samples, respectively, showing a consistent 1% difference between the two process routes. The different characteristics of the densification between DP and CIP samples can be readily explained on the basis of the inter-agglomerate pores present in the green bodies (Fig. 2). The nature of the inter-agglomerate pores are similar between powder-650 and powder-900, which explains the coincident densification between the two powders. The superior densification and higher density of the CIP samples is not only due to the higher green densities for the CIP samples; but most importantly, the CIP samples have a reduced amount and smaller inter-agglomerate porosity than DP samples. The effect of inter-agglomerate porosity on the densification in zirconia ceramics has been widely observed by others [5–7, 18]. There exist large pores remaining in the DP green samples that can remain as the source of the residual pores that were not able to sinter out in the samples fired at 1400 °C.

3.4. Microstructural evolution and grain growth

Fig. 5 shows the microstructures of the samples prepared under different sintering conditions. At a sintering temperature of 1250 °C, the pores were reduced in size with sintering time. The pores exist in the form of continuous open porosity when the dwell time is less than 4 h. As the time increases, the linked pores become smaller and are reduced to closed pores, indicating that the sintering has reached an intermediate stage.

According to dilatometric results, the sintering started as low as 800 °C (see Fig. 3) for the nano-sized zirconia powder compact. Even lower sintering start temperatures have been observed for finer zirconia powder compacts [3, 11]. The initial sintering occurs within agglomerates or particle domains, and the intra-agglomerate pores disappear [3, 5–7, 18, 19]. The shrinkage of each agglomerate results in the growth of inter-agglomerate pores. Further sintering requires the grain growth of sintered parts, and grains and pore rearrangement [19]. Grain growth and/or pore size redistribution phenomena (e.g., Rayleigh-like instability) can

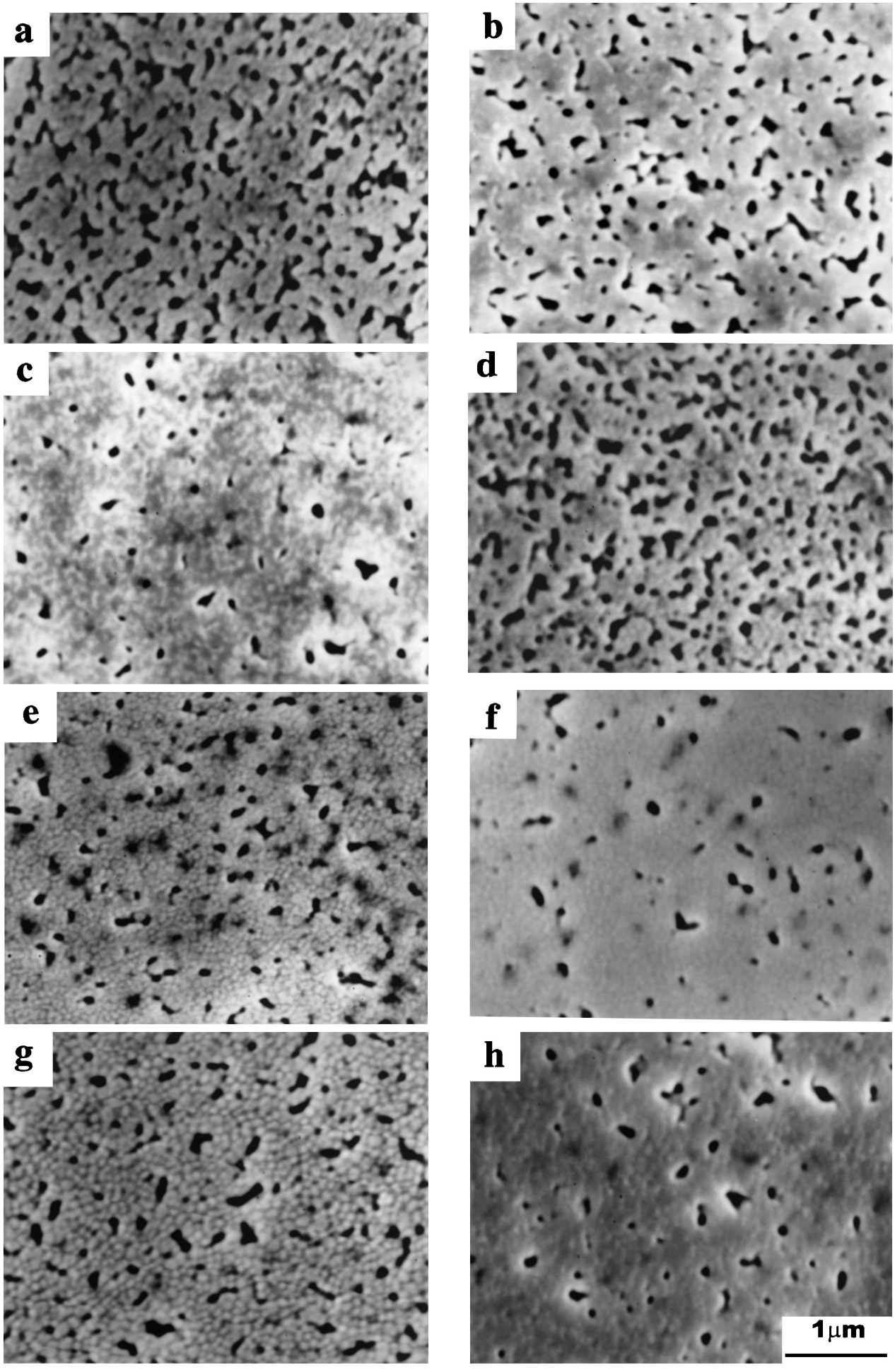

Figure 5 The microstructure evolution during sintering 3Y–TZP ceramics: (a) DP-650 at 1250 °C, 1 h; (b) DP-650 at 1250 °C, 4 h; (c) DP-650 at 1250 °C, 16 h; (d) DP-900 at 1250 °C, 1 h; (e) DP-900 at 1250 °C, 4 h; (f) DP-900 at 1250 °C, 16 h; (g) DP-650 at 1300 °C, 1 h; and (h) DP-650 at 1350 °C, 1 h.

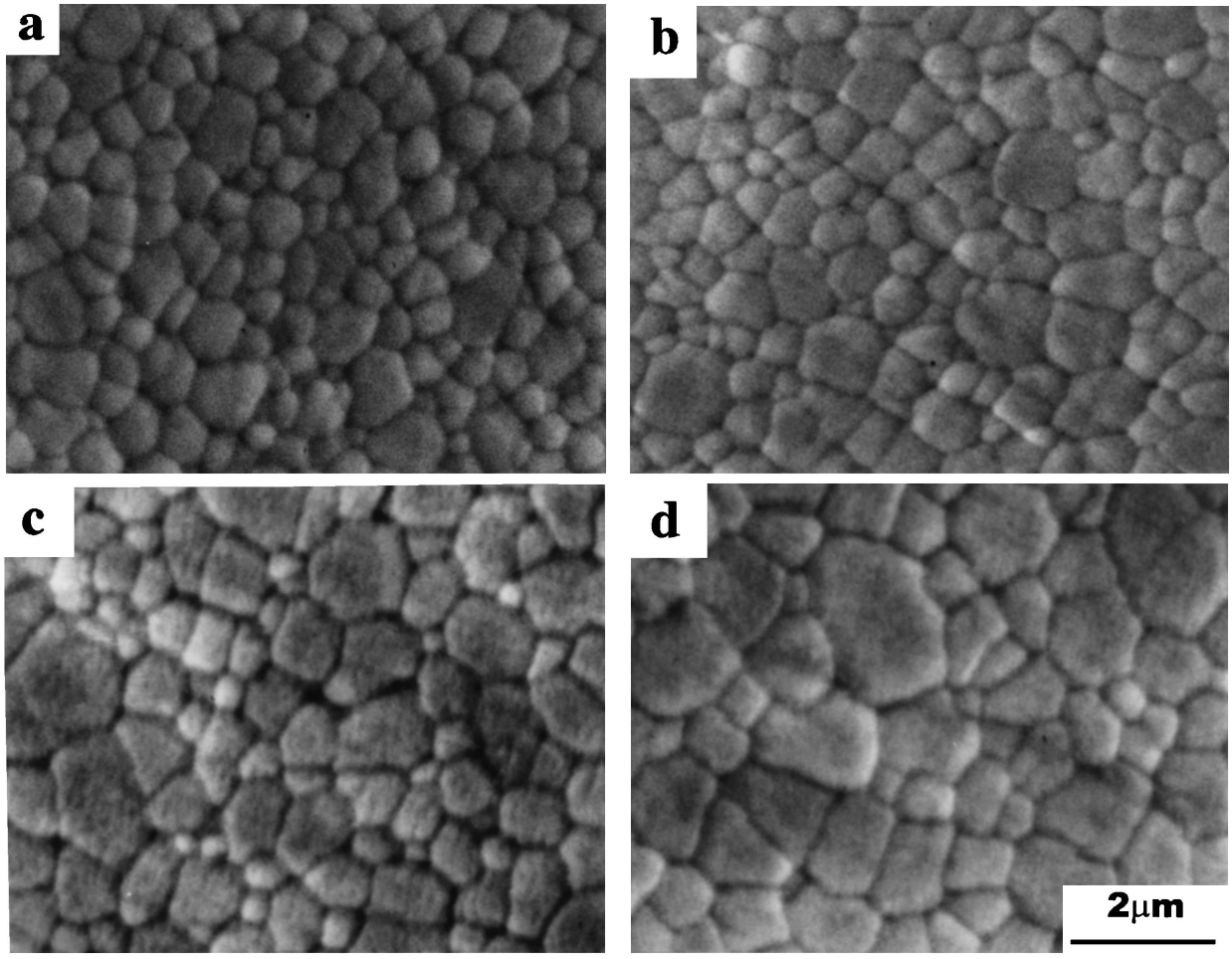

Figure 6 The grain structure of DP-900 sintered at 1400 °C for (a) 2 h; (b) 8 h; (c) 16 h; and (d) 32 h.

decrease the coordination number of remaining pores. It was also noted that grain growth took place during initial sintering of nano-sized zirconia. The grains grew to around 100 nm in size for both powder-650 and powder-900 on sintering at 1250 °C. For longer durations, the sintering was able to reach the second stage, and the intra-agglomerate pores reduced in size and eventually were eliminated at this stage. At higher temperatures (1300 or 1350 °C), the second stage of sintering can be reached in even shorter times. Examination of the microstructure shows that the pores exist in the form of close pores (Fig 5g and h). At even higher temperature and longer dwelling time, the remaining closed pores are eliminated when grain growth becomes a predominant phenomenon. Fig. 6 shows an example of grain growth observed at 1400 °C. Coinciding with the variation in density, a number of large isolated pores were readily observed in DP-650 and DP-900 specimens, but such pores could rarely be found in CIP-650 and CIP-900 specimens. This behavior can be explained by Lange's theory [19]. Where there are large pores remaining in the powder compact of DP-650 and DP-900, these pores cannot be eliminated during standard sintering procedures [18].

Fig. 5 compares the microstructure evolution of powder-650 and powder-900 sintered at 1250 °C. It shows no obvious difference between the two samples. Similar features in the microstructures were notable, such as the morphology and distribution of pores as well as grain size, which can be attributed to the similarity of the inter-agglomerate pores in the green bodies. The similarity in microstructure is also reflected in the similar densification behavior (Fig. 3).

Fig. 7a and b show the effect of sintering temperature and dwell time on the grain size of the 3Y–TZP. The grain growth on sintering at 1250 °C has also been examined. The average grain size is approximately 100 nm, but accurate measurements are difficult due to the fine grain size and high porosity levels. XRD line broadening has been used to monitor grain growth during low-temperature sintering of nano-sized zirconia [2, 15], but this technique is only suitable for a crystallite size below 40 nm; thus, the technique cannot be applied. Nevertheless, SEM micrographs indicated that the grain size is insensitive to dwell time. The lack of grain growth was also observed in the samples sintered at 1300 °C for up to 16 h. In both cases, second-stage sintering is taking place; one might infer that grain growth is limited during the second stage of sintering where the densification is the predominant process. As soon as the sintering reaches the final stage, significant grain growth occurred and was observed at sintering temperatures of 1350 and 1400 °C or at 1300 °C for longer dwell times. The general grain-growth equation for isothermal conditions is [20, 21].

$$G^n - G_o^n = kt \tag{2}$$

where G and G_o are the average grain sizes at time t and o, respectively, and n is a constant, with a value of 1–4,

TABLE I The fitted equations for the grain growth in 3Y–TZP

Temperature	Powder-650	Powder-900
1300 °C	D^3–$0.094^3 = 8.04e{-}4t$	D^3–$0.090^3 = 7.33e{-}4t$
1350 °C	D^3–$0.263^3 = 1.51e{-}3t$	D^3–$0.264^3 = 1.35e{-}3t$
1400 °C	D^3–$0.377^3 = 3.45e{-}3t$	D^3–$0.343^3 = 4.31e{-}3t$

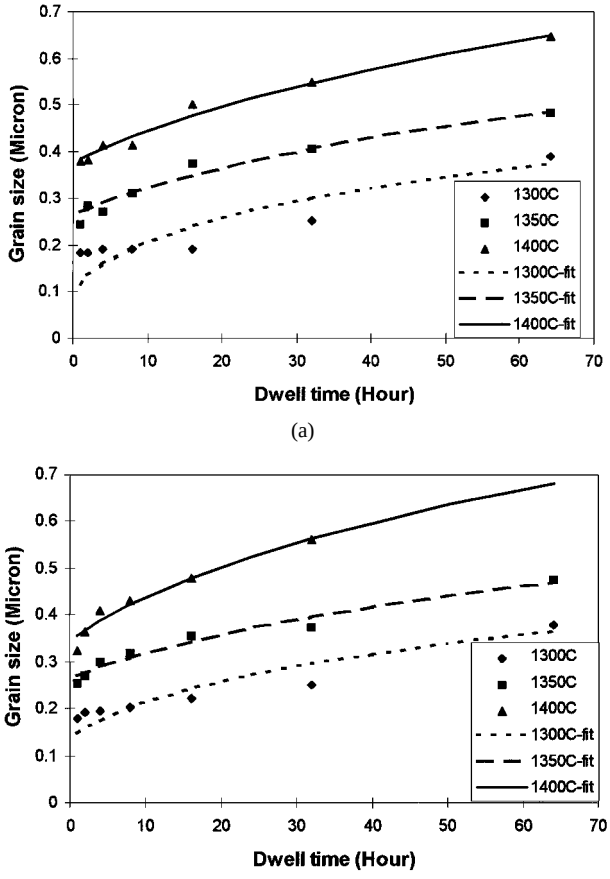

Figure 7 The effect of dwell time on the grain size of 3Y–TZP at three different sintering temperatures: (a) powder-650 and (b) powder-900. The curves were fitted to the experimental results by G^3–$G_O^3 = kt$.

dependent on the rate-controlling diffusion mechanism for the grain growth. In most cases, $n = 3$ for zirconia ceramics [2, 22–24]. Equation 2 was used to fit the grain-growth experimental results, which are listed in Table I, and the fitted curves are shown in Fig. 7. A good fit was obtained, similar to earlier results, with $n = 3$, indicating that the rate-controlling mechanisms for grain growth in zirconia ceramics are lattice diffusion, gas phase diffusion, or impurity drag. Grain growth in zirconia ceramics is usually generated by surface and grain boundary diffusion during the initial stage and solid-solution drag at final stage [2, 17]. A second phase can often be formed on the grain boundary [8, 9] and if Y_2O_3 is present, it can become segregated on the grain boundary [2, 9, 15, 17]. Therefore, in our case, the most likely rate-controlling mechanism for the grain growth is solid-solution drag [2, 17]. The constant, k, in Equation 2 is related to the diffusion rates of the grain growth, D, as follows:

$$k = \alpha D = \beta \exp(-E/RT) \qquad (3)$$

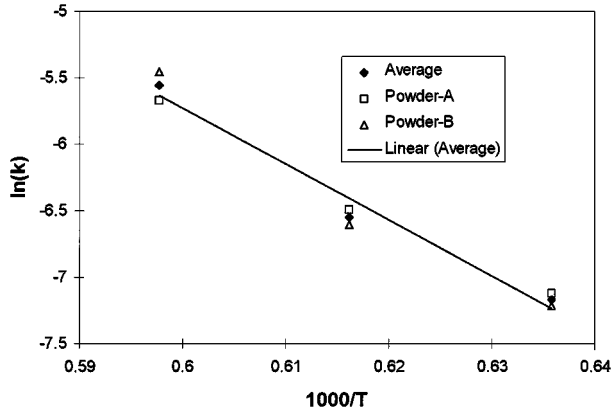

Figure 8 $\ln(k)$ against $1/T$ plot for grain growth.

where α and β are the constants, related to grain boundary energy, atomic volume, and grain boundary thickness; β is also related to the hopping frequency. E is the activation energy for diffusion, T the absolute temperature, and R the gas constant. Hence, the activation energy for diffusion can be obtained by the plot of $\ln(k)$ versus $1/T$, as shown in Fig. 8. The calculated activation energies for the grain growth are 318 kJ/mol for powder-650 and 386 kJ/mol for powder-900. Because the two powders were obtained at different calcination temperature from the same starting powder, and earlier results indicated that the sintering and grain growth mechanisms are the same for both of the powders, the activation energy for grain growth should be the same; the observed difference in the activation energy was thus generated by experimental error. Hence, the average value is used to represent the activation energy for the grain growth in this case, which is 352 kJ/mol. Doped zirconia ceramics (Y_2O_3, CaO–doped) have a high oxygen ionic diffusion rate, and the activation energy for oxygen diffusion in 3Y–TZP ceramics is around 100 kJ/mol, which is much lower than the activation energy for the grain growth. The low diffusion rate of the cation (Zr^{4+}) in zirconia ceramics controls the process of the grain growth; thus, the activation energy for the grain growth is reflected in the activation energy for the cation diffusion. The activation energy obtained in the present study for grain growth is, in fact, similar to the earlier results for the activation energy for cation diffusions: 387 kJ/mol for Zr^{4+} and 421 kJ/mol for Ca^{2+} in $0.16CaO$–$0.84ZrO_2$ ceramics [25]. Sakka [26] measured Zr–Hf interdiffusion coefficient in the solid-solution $0.16Y_2O_3$–$0.84Zr_{1-x}Hf_xO_2$ and found the lattice diffusion energy to be 391 kJ/mol and the grain boundary diffusion energy to be 309 kJ/mol. Table II compares the present results of the activation energy with some earlier results. The values in the present experiments are similar to those measured by the diffusion technique, and lower than those measured by sintering.

4. Discussion

In general, the sinterability of ceramics is closely related to the particle size of the starting powders; finer particles can be sintered at lower temperatures. The

TABLE II The activation energies for cation diffusion and grain growth in zirconia ceramics

Material	Activation Energy (kJ/mol), diffusion	Measurement	Reference
$0.16CaO–0.84ZrO_2$	387, Zr^{4+} 421, Ca^{2+}	Tracer diffusion	[25]
$0.16Y_2O_3–0.84Zr_{1-x}$ Hf_xO_2	391, Lattice 309, Grain boundary	Zr^{4+}–Hf^{4+} Interdiffusion	[26]
3Y–TZP	580, Grain growth	Superplastic	[22]
2.8Y–TZP	615, Grain growth	Sintering	[23]
3Y–TZP	492, Grain growth	Sintering	[24]
3Y–TZP	275, Grain growth 510, Grain growth	Initial stage sintering Final stage sintering	[2]
3Y–TZP	352, Grain growth	Final stage sintering	present study

development of fine and even nano-sized ceramic powder has been and remains a priority for ceramists. However, agglomeration of the powder is often more important, determining both the sintering temperature and the final density. Due to the high surface energy associated with nano-sized powders, agglomerates will inevitably form. Inter-agglomerate pores, as well as intra-agglomerate pores, form in the powder compact. This type of pore of a size similar to the particle size can readily be eliminated at low sintering temperatures. However, the inter-agglomerate pores, which are usually much larger than the powder particle size, cannot be immediately removed. Higher temperatures are required to reduce the coordination number of the pores generated by the grain growth and then to remove them [19]. In the case of a compact of a fully agglomerated powder, the inter-agglomerated pores may well not be eliminated by increasing sintering temperature [18]. In the present study, the sintering behavior is largely unaffected by, and the final density and grain size are almost independent, of the particle size. Therefore, powder morphology and the aggregation could be the major factor controlling behavior. The characteristics developed by the agglomerates are closely related to the powder-processing techniques [5, 7]. Soft agglomerates can be destroyed during the formation of the powder compact, which does not adversely affect densification, but hard agglomerates will result in the formation of the large inter-agglomerate pores in the powder compact, which is not beneficial.

To fabricate high-quality ceramics, control of the grain growth during sintering and thermal treatment is considered essential. It is a requirement for 3Y–TZP ceramics in order to attain strength and toughness to have a uniform sub-micron grain structure. In the initial and intermediate stages of the sintering for 3Y–TZP, the grain size is in the range of 100 to 200 nm, and the grain growth is small. The grain size (100–200 nm) is not a critical factor in reducing mechanical propertis, but the high level of porosity present at this stage would be expected to have a strong influence on the mechanical properties. Full density is usually required to achieve optimum mechanical properties and which the materials would be expected to attain during the final stage of sintering. The occurrence of grain growth is important in determining the properties of the finished ceramic. It can be accepted that the grain-growth mechanism at the final stage of 3Y–TZP is controlled by the solid-solution drag mechanism. Therefore, control of the impurity content or addition of a controlled amount of dopants could be expected to aid control of the grain-growth rate during the final stages of firing. Y^{3+} reacts with the grain boundary phase (impurities and segregated ions) on the grain boundary, often in the form of a liquid phase at sintering temperatures. Abnormal grain growth can then take place to form large cubic grains, especially in the presence of enhanced Y^{3+} concentration due to segregation, in this case when firing at high temperatures for long periods, which causes a reduction in the mechanical properties [27], particularly strength.

5. Conclusions

1. Two kinds of pores, inter- and intra-agglomerate pores, are formed in the green body. Intra-agglomerate pores have only an effect on the initial sintering, but the inter-agglomerate porosity has a major effect on the sintering and final density.

2. During sintering, the grains first grow to approximately 100 nm to reach the intermediate stage of the sintering, when the grain growth rate is reduced prior to as the densification reaches the final stage.

3. At the final stage, significant grain growth was found to have take place. The activation energy for the grain growth is approximately 352 kJ/mol, and the exponent is $n = 3$.

Acknowledgements

One of the authors (S. A.) would like to thank the British Council for the financial support to study at the University of Bath and conduct the research.

References

1. G. SKANDAN, *Nano-struct. Mater.* **5** (1995) 111.
2. G. S. A. M. THEUNISSEN, A. J. A. WINNUBST and A. J. BURGGRAAF, *J. Eur. Ceram. Soc.* **11** (1993) 315.
3. D. C. HAGUE and M. J. MAYO, *J. Am. Ceram. Soc.* **80** (1997) 8149.
4. D. J. CHEN and M. J. MAYO, *ibid.* **79** (1996) 906.
5. M. A. C. G. VAN DE GRAAF, J. H. H. TER MAAT and A. J. BURGGRAAF, in "Advances in Ceramics, Vol. 12," edited

by N. Claussen, M. Ruhle and A. H. Heuer (The American Ceramic Society, Inc., Columbus, Ohio, 1984) pp. 744–765.
6. X. X. JIANG, D. S. HUANG and L. WENG, *J. Mater. Sci.* **29** (1994) 121.
7. A. ROOSEN and H. HAUSNER, in "Advances in Ceramics, Vol. 12," edited by N. Claussen, M. Ruhle and A. H. Heuer (The American Ceramic Society, Inc., Columbus, Ohio, 1984) pp. 714–726.
8. M. RUHLE, N. CLAUSSEN and A. H. HEUER, in "Advances in Ceramics, Vol. 12," edited by N. Claussen, M. Ruhle and A. H. Heuer (The American Ceramic Society, Inc., Columbus, Ohio, 1984) pp. 352–370.
9. T. STOTO, M. NAUER and C. CARRY, *J. Am. Ceram. Soc.* **74** (1991) 2615.
10. S. LAWSON, C. GILL and G. P. DRANSFIELD, *J. Mater. Sci.* **30** (1995) 3057.
11. C. M. J. HWANG and I. W. CHEN, *J. Am. Ceram. Soc.* **73** (1990) 1626.
12. J. R. SEIDENSTICKER and M. J. MAYO, *ibid.* **79** (1996) 401.
13. L. RUIZ and M. J. READEY, *ibid.* **79** (1996) 2331.
14. S. A. NIGHTINGALE, D. P. DUNNE and H. K. WORNER, *J. Mater. Sci.* **31** (1996) 5039.
15. M. M. R. BOUTZ, A. J. A. WINNUBST and A. J. BURGGRAAF, *J. Eur. Cer. Soc.* **13** (1994) 89.
16. M. A. C. G. VAN DE GRAAF, J. H. H. TER MAAT and A. J. BURGGRAAF, *J. Mater. Sci.* **20** (1985) 1407.
17. M. M. R. BOUTZ, C. S. CHEN, A. J. A. WINNUBST and A. J. BURGGRAAF, *J. Am. Ceram. Soc.* **77** (1994) 2632.
18. J. L. SHI, J. H. GAO, Z. X. LIN and T. S. YEN, *ibid.* **74** (1991) 994.
19. F. F. LANGE, *ibid.* **67** (1984) 83.
20. R. J. BROOK "Treatise on Materials Science and Technology, Vol 9," Edited by F. F. Y. Wang (Academic Press, New York, 1976) pp. 331–364.
21. T. A. RING (ed), "Fundamentals of Ceramic Powder Processing and Synthesis (Academic Press, San Diego, California, 1996) pp. 827–830.
22. T. G. NIEH and J. WADSWORTH, *J. Am. Ceram. Soc.* **72** (1989) 1469.
23. J. WANG and R. RAJ, *ibid.* **74** (1991) 1959.
24. F. WAKAI, Y. KADAMA, S. SAKORGUCHI, M. MURAYAMA, H. KATO and T. NAGONE, in "Proceedings of the MRS International Meeting on Superplasticity, Vol. 7" (Materials Research Society, Pittsburgh, Pennsylvania 1989) pp. 259.
25. W. H. RHODES and R. E. CARTER, *J. Am. Ceram. Soc.* **49** (1966) 244.
26. Y. SAKKA, Y. IOSHI and K. ANDO, *J. Mater. Sci.* **17** (1982) 3101.
27. L. MONTANARO, L. FERRONI, S. PAGLIOLICO, M. V. SWAIN and T. J. BELL, *J. Am. Ceram. Soc.* **79** (1996) 1034.

Received 7 July
and accepted 17 August 1998